Voltage- and calcium-dependent gating of TMEM16A/Ano1 chloride channels are physically coupled by the first intracellular loop

Qinghuan Xiao[a], Kuai Yu[a], Patricia Perez-Cornejo[b], Yuanyuan Cui[a], Jorge Arreola[c], and H. Criss Hartzell[a,1]

[a]Department of Cell Biology, Emory University School of Medicine, Atlanta, GA 30322 and [b]School of Medicine and [c]Physics Institute, Universidad Autónoma de San Luis Potosí, San Luis Potosí, SLP 78290, Mexico

Edited by David E. Clapham, Children's Hospital Boston, Howard Hughes Medical Institute, Boston, MA, and approved April 11, 2011 (received for review February 8, 2011)

Ca^{2+}-activated Cl^- channels (CaCCs) are exceptionally well adapted to subserve diverse physiological roles, from epithelial fluid transport to sensory transduction, because their gating is cooperatively controlled by the interplay between ionotropic and metabotropic signals. A molecular understanding of the dual regulation of CaCCs by voltage and Ca^{2+} has recently become possible with the discovery that Ano1 (TMEM16a) is an essential subunit of CaCCs. Ano1 can be gated by Ca^{2+} or by voltage in the absence of Ca^{2+}, but Ca^{2+}- and voltage-dependent gating are very closely coupled. Here we identify a region in the first intracellular loop that is crucial for both Ca^{2+} and voltage sensing. Deleting $_{448}$EAVK in the first intracellular loop dramatically decreases apparent Ca^{2+} affinity. In contrast, mutating the adjacent amino acids $_{444}$EEEE abolishes intrinsic voltage dependence without altering the apparent Ca^{2+}affinity. Voltage-dependent gating of Ano1 measured in the presence of intracellular Ca^{2+} was facilitated by anions with high permeability or by an increase in $[Cl^-]_e$. Our data show that the transition between closed and open states is governed by Ca^{2+} in a voltage-dependent manner and suggest that anions allosterically modulate Ca^{2+}-binding affinity. This mechanism provides a unified explanation of CaCC channel gating by voltage and ligand that has long been enigmatic.

allosteric mechanism | chloride channel | patch clamp

Ca^{2+}-activated Cl^- channels (CaCCs) play manifold roles in cell physiology (1, 2), including epithelial secretion (3, 4), sensory transduction and adaptation (5–8), regulation of smooth muscle contraction (9), control of neuronal and cardiac excitability (10), and nociception (11). This myriad of functions has attracted attention for more than 25 years (12, 13), but a lack of consensus regarding their molecular composition has stymied a mechanistic understanding of their gating. Recently, two members of the TMEM16/anoctamin family (Ano1 and Ano2) were identified as CaCC channels (14–16) and shown to be essential for salivary exocrine secretion (14, 17, 18), gut slow-wave activity (18, 19), tracheal secretion (18, 20, 21), and olfactory transduction (5–7).

Ano1 and Ano2 are well suited for their diverse roles because they are dually gated by voltage (V_m) and intracellular Ca^{2+} concentration ($[Ca^{2+}]_i$), so that their activity is tuned by the interplay between metabotropic and ionotropic inputs (14, 16, 22–24). The molecular mechanisms underlying V_m and Ca^{2+} gating are unknown, however. Unlike typical V_m-gated channels or ligand-gated channels, CaCCs exhibit both V_m dependence and ligand gating that are strongly coupled and apparently reciprocally related. Ano1 does not contain obvious V_m-sensing or Ca^{2+}-sensing domains (14). Because Ca^{2+} is often stabilized in proteins by oxygen atoms (25), it seemed reasonable to hypothesize that acidic amino acids contribute to the Ca^{2+}-binding site. Ca^{2+} sensors in two other Ca^{2+}-activated channels, BK and Best1, are associated with sequences rich in acidic amino acids (26, 27). The Ano1 sequence has a similar domain in the first intracellular loop (amino acids 430–480), composed of residues $_{444}$EEEEEAVK$_{451}$ (Fig. S1). Here we show that this region plays a key role in transducing both V_m and Ca^{2+} signals.

Results

Voltage and Ca^{2+} Synergistically Gate Ano1. At low $[Ca^{2+}]_i$ (<1 μM), WT Ano1 (splice variant **a,c**) was activated synergistically by Ca^{2+} and depolarization. In the absence of Ca^{2+}, no current was evident at V_m between −100 mV and +100 mV, but as $[Ca^{2+}]_i$ was increased, an outward current was activated by depolarization and deactivated by hyperpolarization (Fig. 1 *A–D* and *F*). As $[Ca^{2+}]_i$ was increased, outward rectification (Fig. 1*F*) and the fraction of total current exhibiting time-dependence (Fig. 1*E*) were reduced. V_m-dependent activation of Ano1 was evaluated by plotting normalized conductance versus V_m (G/G_{max} vs. V_m curves; Fig. 1*G*). The data were well fit by the Boltzmann equation,

$$G/G_{max} = 1/\left\{1 + \exp\left[(V_m - V_{0.5})z\,F/RT\right]\right\},$$

where G/G_{max} is normalized conductance; z is the equivalent gating charge associated with voltage-dependent channel opening; $V_{0.5}$ is the membrane potential (V_m) where G/G_{max} is half-maximal and is related to the conformational energy associated with voltage-independent channel opening; and F/RT = 0.039 mV^{-1}. At 1 μM Ca^{2+}, $V_{0.5}$ was 64 ± 0.9 mV (Fig. 1*G*, black squares); doubling $[Ca^{2+}]$ to 2 μM shifted the G/G_{max} vs. V_m curve to the left by −145 mV (Fig. 1*G*, red circles) with no significant effect on z. Because Ca^{2+} shifts the G/G_{max} vs. V_m curves so dramatically, a complete G/G_{max} vs. V_m curve could be recorded for only a narrow range of $[Ca^{2+}]_i$. For these $[Ca^{2+}]$, z was not obviously Ca^{2+}-dependent (z = 0.40–0.46). This indicates that Ca^{2+} does not change the V_m sensitivity (z) of the Ano1 channel, but rather shifts $V_{0.5}$, the energy associated with V_m-independent gating.

Although these data may imply that Ano1 is a simple ligand-gated channel, Ano1 is actually more complicated, because Ca^{2+} gating is strongly influenced by V_m. The EC_{50} of Ano1 for Ca^{2+} decreases ~15-fold from 5.9 ± 2.5 μM at −100 mV to 0.4 ± 0.1 μM at +100 mV while the Hill coefficient, n_H, indicative of the cooperativity of Ca^{2+} binding, increases from 1.0 ± 0.1 to 2.0 ± 0.4 (Fig. 1 *H* and *I*). These data support a mechanism of Ano1 gating with V_m and Ca^{2+} converging on the switch between closed and open conformations.

Glutamic Acids in the First Intracellular Loop Contribute to Channel Gating. The first intracellular loop of Ano1 contains five consecutive glutamic acids ($_{444}$EEEEE$_{448}$), resembling the "Ca^{2+} bowl" of BK channels (26) and the acidic cluster in hBest1 (27) that are linked to Ca^{2+} sensing (Fig. S1). The last glutamic acid

Author contributions: Q.X., K.Y., P.P.-C., J.A., and H.C.H. designed research; Q.X., K.Y., Y.C., J.A., and H.C.H. performed research; Q.X., K.Y., P.P.-C., Y.C., J.A., and H.C.H. analyzed data; and Q.X., K.Y., P.P.-C., J.A., and H.C.H. wrote the paper.

The authors declare no conflicts of interest.

This article is a PNAS Direct Submission.

[1]To whom correspondence should be addressed. E-mail: criss.hartzell@emory.edu.

This article contains supporting information online at www.pnas.org/lookup/suppl/doi:10.1073/pnas.1102147108/-/DCSupplemental.

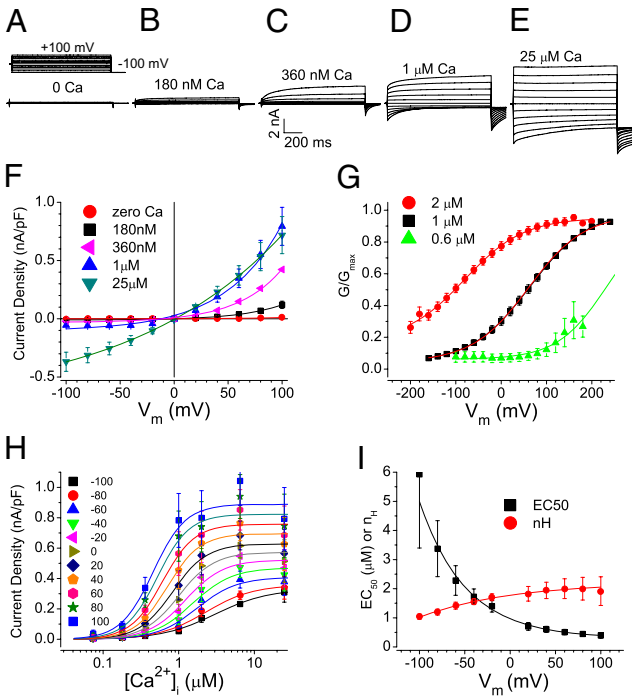

Fig. 1. WT Ano1 gating by voltage and Ca^{2+}. (*A–E*) Representative $I_{Cl,Ano1}$ in transfected HEK293 cells at the indicated free $[Ca^{2+}]$. Voltage protocol is shown above *A*. (*F*) Steady-state current–voltage relationships (n = 5–9). (*G*) G/G_{max} vs. V_m curves for Ano1 in excised patches activated by 0.6 μM (▲), 1 μM (■), and 2 μM (●) Ca^{2+}. (*H*) Instantaneous tail current density at −100 mV after prepulses to V_m plotted vs. free $[Ca^{2+}]$ and fitted to the Hill equation. (*I*) EC_{50} (■) and n_H (●) values from fits in *H* plotted vs. V_m.

of this cluster, $_{448}$E, is the first residue of a naturally occurring alternatively spliced segment, $_{448}$EAVK$_{451}$ (28). To investigate this region in detail, we mutated the first four glutamic acids to alanines ($_{444}$EEEE/AAAA$_{447}$) and deleted $_{448}$EAVK$_{451}$ (ΔEAVK) (current traces; Fig. S2). The ΔEAVK deletion and, to a lesser extent, the $_{444}$EEEE/AAAA$_{447}$ mutation, shifted G/G_{max} vs. V_m curves at each $[Ca^{2+}]_i$ to the right without altering the slope (Fig. 2). For ΔEAVK, the position of the G/G_{max} vs. V_m curve on the V_m axis was relatively insensitive to Ca^{2+}: 2 μM Ca^{2+} had no effect, and 25 μM Ca^{2+} shifted the curve only to a position comparable to the WT curve at 1 μM Ca^{2+}. The slope of the relationship between $V_{0.5}$ and $[Ca^{2+}]_i$ was reduced ~50-fold for ΔEAVK and ~3-fold for $_{444}$EEEE/AAAA$_{447}$ compared with WT (Fig. 2*C*). Because $V_{0.5}$ represents the conformational energy associated with V_m-independent channel opening, these mutations decrease the ability of Ca^{2+} to reduce the activation energy required for the channel to open. This could be caused by either lower Ca^{2+}-binding affinity or decreased stability of the Ca^{2+}-bound open state.

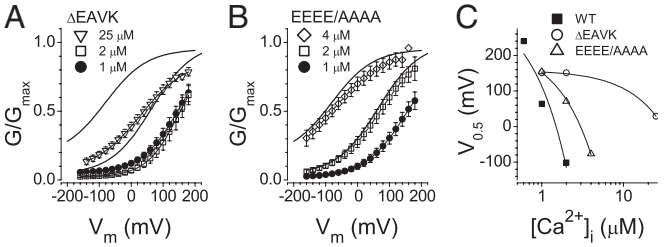

Fig. 2. G/G_{max} vs. V_m curves for mutant Ano1 in excised patches at the indicated $[Ca^{2+}]_i$. (*A* and *B*) Solid lines without symbols: WT from Fig. 1*G* at 1 μM and 2 μM Ca^{2+}. (*A*) ΔEAVK with 25 μM (▽), 2 μM (□), and 1 μM (●) Ca^{2+}. (*B*) $_{444}$EEEE/AAAA$_{447}$ with 25 μM (◇), 2 μM (□), and 1 μM (●) Ca^{2+}. (*C*) $V_{0.5}$ vs. $[Ca^{2+}]$ for WT (■), ΔEAVK (○), and $_{444}$EEEE/AAAA$_{447}$ (△).

Ca^{2+} Dissociation Is V_m-Dependent and Slow. To test whether these mutations alter Ca^{2+} affinity, we performed fast perfusion experiments in which excised patches were switched between zero and high $[Ca^{2+}]$ within several ms (Fig. S3). Fig. 3 displays examples of the time course of Ano1 activation at the indicated V_m when Ca^{2+} was increased rapidly from 0 μM to 20 μM (Fig. 3*A*) and deactivation when Ca^{2+} was withdrawn (Fig. 3*B*). The time course of activation was sigmoid and displayed a lag period consistent with multistep channel opening. For simplicity, current activation after the initial lag period was fit to a monoexponential equation to calculate the time constant of activation, τ_{on} (Fig. 3*A*). τ_{on} was decreased when $[Ca^{2+}]$ was increased, as expected if Ca^{2+} binding is a rate-limiting step in channel opening. τ_{on} was not strongly V_m-dependent (Fig. 3*E*). On removal of Ca^{2+}, the currents decayed monoexponentially (Fig. 3*B*), and τ_{off} was strongly V_m-dependent, with an e-fold slowing per 70.3-mV depolarization for WT (Fig. 3*F*). $_{444}$EEEE/AAAA$_{447}$ and ΔEAVK mutations had no significant effect on τ_{on} (Fig. 3*E*). In contrast, τ_{off} was greatly accelerated by ΔEAVK and slightly accelerated by the $_{444}$EEEE/AAAA$_{447}$ mutation at positive V_m (Fig. 3*F*). At +120 mV, τ_{off} was 501.5 ± 10.2 ms for WT, 37.4 ± 1.1 ms for ΔEAVK, and 345.0 ± 18.8 ms for $_{444}$EEEE/AAAA$_{447}$. Because τ_{off} for WT was surprisingly slow, for comparison, we performed an experiment using patches containing the BK Ca^{2+}-activated K^+ channel (Fig. S3). τ_{off} for the BK channel was 28 ms, ~20-times faster than for WT Ano1.

τ_{off} is equal to the reciprocal of the rate constant(s) of the rate-limiting step(s) leading to channel closure, which could be Ca^{2+} dissociation or channel closure itself. As a test of the idea that τ_{off} reflects ligand dissociation, we measured τ_{off} for Ba^{2+}-activated Ano1. Because the free energy of hydration of Ba^{2+} is smaller than that of Ca^{2+}, Ba^{2+} binding to sites composed of coordinating oxygen ligands is significantly less stable than that of Ca^{2+} (25). For example, Ba^{2+} is almost inactive in activating CaM-dependent phosphodiesterase or displacing Ca^{2+} from CaM (29). The apparent EC_{50} for Ano1 activation is >10-fold larger for Ba^{2+} than for Ca^{2+}, reflected as a 20-fold faster turnoff of the Ano1 current on Ba^{2+} washout (Fig. 3 *I* and *J*). These observations support the conclusion that τ_{off} reflects ligand dissociation and, therefore, ΔEAVK dramatically increases the rate of Ca^{2+} dissociation from the channel at all voltages.

Assuming that the rate-limiting steps are Ca^{2+} binding and unbinding, the apparent EC_{50} for Ca^{2+} can be calculated as

$$EC_{50} = \alpha/\beta, \text{ where } \alpha = 1/\tau_{off} \text{ and } \beta = \{(1/\tau_{on})-\alpha\}[Ca^{2+}].$$

Deletion of EAVK produces a large increase in EC_{50} at all voltages (Fig. 3*G*), suggesting an important role in Ca^{2+} sensing. In contrast, $_{444}$EEEE/AAAA$_{447}$ is similar to WT. The V_m-dependence of EC_{50} is well described by the equation

$$EC_{50} = EC_{50(0mV)} \cdot \exp(-z\delta FV_m/RT),$$

where $EC_{50(0mV)}$ is the EC_{50} value at 0 mV, z = 2, and δ is the electric field fraction (Fig. 3*G*). The $EC_{50(0mV)}$ values were 1.39 μM for WT and 71 μM for ΔEAVK. Values of δ were similar, 0.16 for WT and 0.12 for ΔEAVK. The V_m dependence of the EC_{50} values agree with other published data for both Ano1 and endogenous CaCCs (14, 22, 23, 28).

Both the Ca^{2+}-activated and the Ba^{2+}-activated currents exhibit a sigmoid onset (Fig. 3 *A* and *H*), indicating that current activation is a highly cooperative multistep process. The sigmoid onset is more pronounced with Ba^{2+}, and the activation, especially the lag period after switching to Ba^{2+} before the current begins to increase, is distinctly V_m-dependent. This V_m dependence is not as obvious with Ca^{2+}, but does appear to be present (Fig. 3*A*). The V_m-dependent sigmoid onset of the current supports a multistep model of Ano1 activation with V_m altering the affinity of the ligand-binding site.

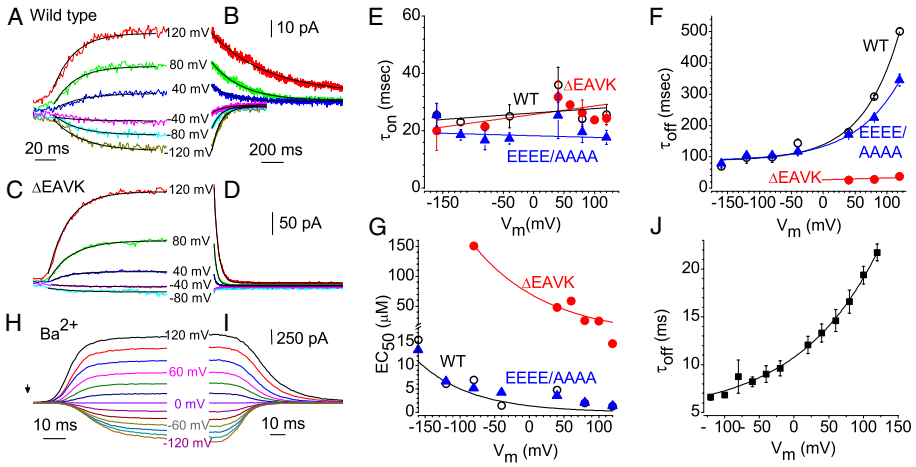

Fig. 3. Activation and deactivation kinetics of Ano1 with rapid Ca^{2+} and Ba^{2+} perfusion. (*A–D*) Representative traces of $I_{Cl,Ano1}$ in response to application (*A* and *C*) and washout (*B* and *D*) of 20 μM Ca^{2+} at the indicated holding potentials. (*A* and *B*) WT Ano1. (*C* and *D*) ΔEAVK. (*E–G*) V_m dependence of τ_{on}, τ_{off}, and EC_{50} for WT Ano1 (○), $_{444}$EEEE/AAAA$_{447}$ (▲), and ΔEAVK (●). (*H* and *I*) Representative traces of increase in current on application (*H*, arrowhead) and washout (*I*) of 1 mM Ba^{2+} (1 mM Ba^{2+}, 100 μM EGTA) for WT Ano1. (*J*) τ_{off} for Ba^{2+}.

The V_m dependence of τ_{off} supports the idea that Ca^{2+} binding is V_m-dependent. If this were the case, then we would expect current deactivation produced by hyperpolarization to reflect Ca^{2+} dissociation as a result of a V_m-dependent decrease in Ca^{2+} affinity. Consequently, we predict that the time constant of current deactivation (τ_{deact}) would become faster with hyperpolarization but slower with increased $[Ca^{2+}]$. This is indeed what we observe (Fig. 4*A*). Consistent with the rapid perfusion, ΔEAVK displays a faster τ_{deact} at each $[Ca^{2+}]$ tested (Fig. 4*B*). A smaller effect is observed with $_{444}$EEEE/AAAA$_{447}$ (Fig. 4*C*).

Ano1 Exhibits Intrinsic Voltage Dependence. Although there are no obvious classical V_m-sensor domains in the predicted transmembrane segments of Ano1 (Fig. S1), Ano1 can be opened by V_m in the absence of Ca^{2+} or other divalent cations by strong depolarization (Fig. 5). Under several conditions with zero $[Ca^{2+}]_i$, depolarizations >100 mV evoke outward currents (Fig. 5 *A*, *D*, and *E*). The magnitude of the Ca^{2+}-independent current was ~100 pA/pF at +200 mV which is <10% that activated by maximum $[Ca^{2+}]_i$ (Fig. 1*H*). The Ca^{2+}-independent currents are mediated by Ano1 because they are not present in HEK cells transfected with GFP alone.

To investigate the role of acidic residues in the Ca^{2+}-independent current, $_{444}$EEEEEAVKD$_{452}$ was deleted. These channels were not activated by depolarizations to +200 mV (Fig. 5*E*), but were activated by Ca^{2+} with an EC_{50} of 45 μM. $_{444}$EEEE/AAAA channels were not activated by V_m either (Fig. 5 *B* and *E*), despite the fact that their Ca^{2+} sensitivity was similar to that of WT. In contrast, ΔEAVK channels were activated more readily by depolarization compared with WT (Fig. 5 *C* and *E*). Taken together, Figs. 2–5 argue that $_{444}$EEEE$_{447}$ and $_{448}$EAVK$_{451}$ are critical in both Ca^{2+}-dependent and V_m-dependent gating of Ano1. The reciprocal relationship of Ca^{2+} and V_m is illustrated by the disruption of $_{448}$EAVK$_{451}$, which decreases apparent Ca^{2+} affinity while stabilizing the V_m-gated open state. The $_{444}$EEEE$_{447}$ mutation, on the other hand, seems to stabilize the closed states of both ligand-gated and voltage-gated pathways.

Voltage Gating Is Affected by Permeant Anions. The observation that neutralization of $_{444}$EEEE$_{447}$ does not change the slope of the G/G_{max} vs. V_m curve (Fig. 2) argues that these residues are not themselves the voltage sensor. Because previous observations showing that the gating of CaCCs in *Xenopus* oocytes and salivary glands is affected by permeant anions (30, 31), we tested the idea that Ano1 voltage sensitivity is related to occupancy of the pore by anions. Replacement of external Cl^- with NO_3^- greatly reduced V_m-dependent gating of Ano 1, as evidenced by a reduction in outward rectification and an increase in the fraction of current activating instantaneously with depolarization (Fig. 6 *A–D*). Furthermore, G/G_{max} vs. V_m curves were shifted to negative potentials when Cl^- was replaced by NO_3^- or SCN^- (Fig. 6 *E* and *F*). These ions would be expected to exhibit a higher occupancy in the pore than Cl^-, because they have lower hydration energies and higher relative permeabilities than Cl^- (31).

If channel gating is dependent on pore occupancy by permeant anions, V_m dependence would be expected to depend on $[Cl^-]$. As expected, increasing $[Cl^-]_e$ shifts the G/G_{max} vs. V_m curves to more negative potentials (Fig. 6*G*). Furthermore, the reversal potential of the current carried by mixtures of Cl^- and I^- cannot be described by the Goldman–Hodgkin–Katz equation (Fig. 6*H*), supporting the idea that channel gating is dependent on ion permeation.

Discussion

The gating of Ano1 is controlled by a complex interplay among $[Ca^{2+}]_i$, V_m, and permeant anions. The most important contribution to gating is provided by an increase in $[Ca^{2+}]_i$ under our conditions. At high concentrations, Ca^{2+} alone is able to open the channel even at very hyperpolarized potentials; however, at lower $[Ca^{2+}]$, voltage has a significant effect that is likely physiologically relevant (see below).

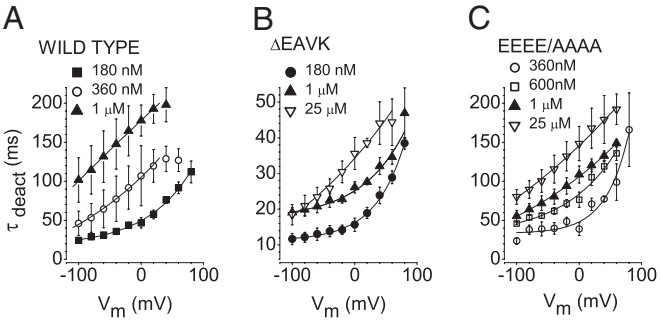

Fig. 4. Deactivation of $I_{Cl,Ano1}$. (*A–C*) V_m and $[Ca^{2+}]$ dependence of tail current deactivation. Currents were activated using a +100-mV pulse, and tail currents were measured at the indicated potentials on the *x*-axis. (*A*) WT Ano1. (*B*) ΔEAVK. (*C*) $_{444}$EEEE/AAAA$_{447}$. n = 4–6.

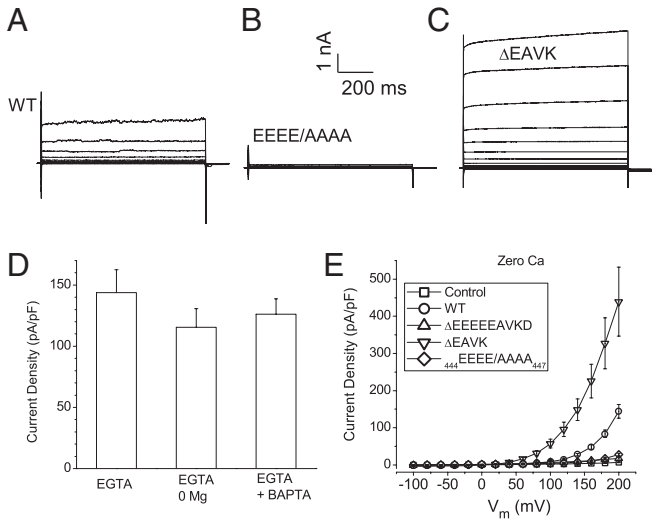

Fig. 5. Activation of Ano1 in zero intracellular Ca^{2+}. (*A–C*) Representative traces of WT Ano1 (*A*), $_{444}$EEEE/AAAA$_{447}$ (*B*), and ΔEAVK (*C*) activated by V_m in nominally zero Ca^{2+}. (*D*) Mean current density at +200 mV with zero intracellular Ca^{2+} plus 5 mM EGTA, zero intracellular Ca^{2+} and Mg^{2+} plus 5 mM EGTA (EGTA + 0 Mg), or zero Ca^{2+} plus 5 mM EGTA plus 1 mM BAPTA in both intracellular and extracellular solutions (EGTA + BAPTA). n = 5–11. (*E*) Steady-state I-V curve from cells dialyzed with zero Ca^{2+}: nontransfected cells (control; □), WT Ano1 (●), Δ_{444}EEEEEAVKD$_{452}$ (△), ΔEAVK (▽), and $_{444}$EEEE/AAAA$_{447}$ (◇). (n = 4–11).

Although Ano1 resembles ligand-gated channels, its V_m sensitivity is unique. For example, Ano1 differs from the ligand-gated nAChR because although nAChR is weakly V_m-sensitive, its affinity for ACh is not obviously V_m-sensitive (32), whereas the Ca^{2+} sensitivity of Ano1 is clearly V_m-sensitive. Furthermore, unlike nAChRs, Ano1 can be completely closed by hyperpolarization in the presence of <1 μM Ca^{2+} and can be opened by strong depolarization itself in the absence of Ca^{2+}. The observation that the channel can be opened in the absence of Ca^{2+} supports the conclusion that the "V_m sensor" is unlikely to be Ca^{2+} itself. Ano1 also differs significantly from the large-conductance Ca^{2+}-activated K^+ channel (BK), in that Ano1 has much higher sensitivity to Ca^{2+} and does not have an obvious protein-based V_m sensor.

Ca^{2+} and V_m Dependence Are Coupled by the First Intracellular Loop. Residues $_{444}$EEEEEAVK$_{451}$ are involved in the transduction of both Ca^{2+} and V_m signals. Deletion of $_{448}$EAVK$_{451}$ severely decreases Ca^{2+} sensitivity and shifts $V_{0.5}$ values to positive voltages. Because $V_{0.5}$ represents the energy of V_m-independent channel opening, ΔEAVK apparently increases the activation energy required for Ca^{2+} to gate the channel open. This could be caused by decreased Ca^{2+}-binding affinity or diminished stability of the Ca^{2+}-bound open state. Colquhoun (33) discussed the difficulty in separating the effects of mutations on channel gating and on ligand binding; however, our fast perfusion experiments provide strong support for a major effect of ΔEAVK on Ca^{2+} binding. Nonetheless, there are several reasons why $_{444}$EEEEEAVK$_{451}$ is unlikely to form part of the Ca^{2+}-binding site. At very positive voltages, the EC_{50} values of WT and ΔEAVK appear to be convergent (Fig. 3*G*), which would not be expected if ΔEAVK disrupted the Ca^{2+}-binding site. Second, neutralizing $_{444}$EEEE$_{448}$ has little effect on apparent Ca^{2+} sensitivity, but renders the channels insensitive to V_m activation in the absence of Ca^{2+} and shifts the G/G_{max} vs. V_m curve to positive potentials in the presence of Ca^{2+}. This suggests that $_{444}$EEEE$_{447}$ is involved in transducing depolarization to channel opening, but is unlikely to contribute to Ca^{2+} binding.

The V_m dependence of the EC_{50} values can result if depolarization drives Ca^{2+} into a binding site within the electrical field or alters binding site conformation and Ca^{2+} affinity. The hypothesis that V_m alters binding affinity is supported by the observation that the V_m dependence of current activation and deactivation in rapid perfusion experiments is different for Ca^{2+} and Ba^{2+} (e.g., a 70 mV/e-fold change in τ_{off} for Ca^{2+}, compared with 115 mV for Ba^{2+}; Fig. 3), whereas electrophoretic effects should be similar, because these ions have similar ionic mobilities (119 $cm^2{\cdot}\Omega^{-1}{\cdot}M^{-1}$ for Ca^{2+} vs. 127 $cm^2{\cdot}\Omega^{-1}{\cdot}M^{-1}$ for Ba^{2+}).

Permeant anions control V_m-dependent gating of native CaCCs in *Xenopus* oocytes and parotid acinar cells (30, 31), as well as other Cl^- channels like ClC-2 (34). Permeant anions also affect Ano1 gating, and we surmise that permeant anion occu-

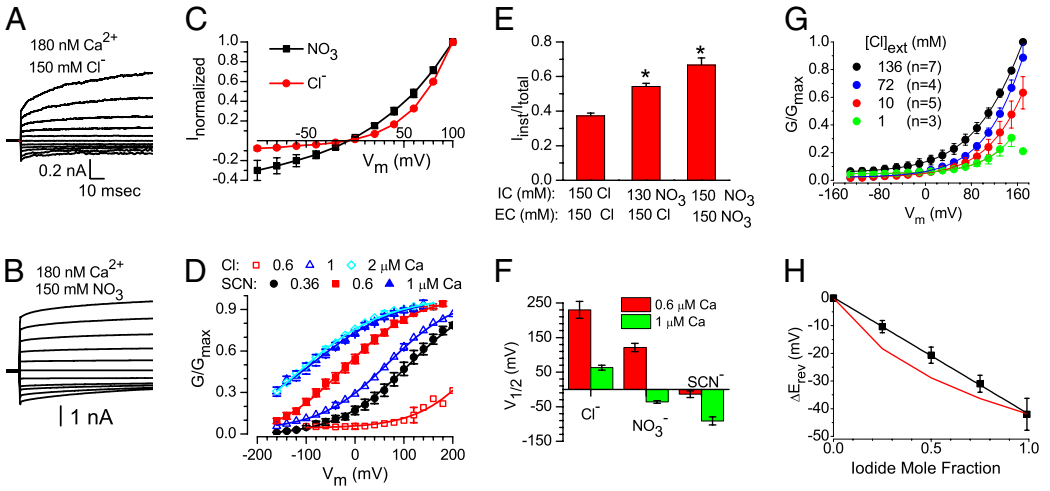

Fig. 6. WT Ano1 gating is dependent on permeant anions. (*A* and *B*) Current traces from a cell dialyzed with 180 nM Ca^{2+} and bathed in symmetrical 150 mM Cl^- (*A*) or 150 mM NO_3^- (*B*). (*C*) Fraction of instantaneous current relative to total current at the end of a 700-ms pulse to +100 mV. (*D*) Normalized (at +100 mV) I-V curves with Cl^- (●) or NO_3^- (■) as permeant ions. (*E*) G/G_{max} vs. V_m curves for WT Ano1 activated at different $[Ca^{2+}]_i$ with Cl^- (open symbols) or SCN^- (filled symbols) as permeant anions. Circles represent 360 nM Ca^{2+}; squares, 600 nM Ca^{2+}; triangles, 1 μM; diamonds, 2 μM. (*F*) $V_{0.5}$ determined from G/G_{max} vs. V_m curves for Cl^-, NO_3^-, and SCN^-. Red bars represent 0.6 μM Ca^{2+}; green bars, 1 μM Ca^{2+}. n = 4–11. (*G*) Cl^- dependence of G/G_{max} vs. V_m curves. $[Cl^-]_e$: 1 mM (green), 10 mM (red), 72 mM (blue), and 136 mM (black). (*H*) Anomalous mole fraction behavior of WT Ano1. The change in E_{rev} is plotted as a function of the mole fraction of iodide (with the balance Cl^-). The red line represents the prediction from the Goldman–Hodgkin–Katz equation.

pancy of the pore stabilizes the open state and thereby allosterically modulates Ca^{2+}-dependent gating. Channel rectification and V_m-dependent gating can be explained by asymmetric access of permeant anions to a critical site in the pore.

We hypothesize that V_m-dependent Ca^{2+} binding may confer a majority of V_m dependence. Simple models with a V_m-dependent Ca^{2+} affinity can reproduce the Ano1 current (22, 23), but allosteric models, such as those used to explain the gating of BK channels (35, 36), are likely to be more successful in explaining the intricate gating of Ano1. However, more structural information is needed about the number of Ca^{2+}-binding sites, the oligomerization state (37, 38), and the involvement of CaM (39). The first intracellular loop of Ano1 is very hydrophilic and unlikely to be located within the transmembrane voltage field (Fig. S1) (40). The physical relationship of $_{444}$EEEEEAVK$_{451}$ to the Ca^{2+}-binding site(s) and the pore, proposed to be in the reentrant loop between transmembrane domains 5 and 6 (14, 15), remains to be determined.

Ano1 Splice Variants and the Role of Calmodulin. Human Ano1 has four different alternatively spliced segments, ***a***, ***b***, ***c***, and ***d***, corresponding to an alternative initiation site, exon-6b, exon-13, and exon-15 (28). Segments ***a*** and ***b*** are located in the N terminus, and segments ***c*** and ***d*** are in the first intracellular loop. Ferrera et al. (28) concluded that deleting segment **c** (ΔEAVK) in human Ano1 affects V_m dependence, but not Ca^{2+} sensitivity. This discrepancy with our conclusion is explained by our observation that ΔEAVK channels are strongly activated by V_m in the absence of Ca^{2+} (Fig. 5). Thus, the current amplitudes reported by Ferrera et al. (28) include both Ca^{2+}-dependent and Ca^{2+}-independent components. The EC_{50} of ΔEAVK channels measured by voltage steps in the presence of steady $[Ca^{2+}]$ will be contaminated by a Ca^{2+}-independent component that will make the EC_{50} appear smaller than it actually is. In contrast, our fast perfusion experiments determine only the Ca^{2+}-dependent component. This difference in methodology likely explains the discrepancy, but differences between human Ano1(***a,b***) and mouse Ano1(***a***) also could play a part.

A recent paper reported that CaM binds to a 22-aa region, CaM-BD1, that overlaps with the ***b*** segment and is essential for gating Ano1(***a,b,c***) (39). However, Tian et al. (39) showed that, unlike Ano1(***a,b,c***), Ano1(***a,c***), which lacks CaM-BD1, does not require CaM. Also, our finding that Ano1(***a,c***) is activated by Ba^{2+} supports a direct effect of Ca^{2+} on Ano1(***a,c***), because CaM is not significantly activated by Ba^{2+} (29). Some endogenous CaCCs are regulated directly by Ca^{2+}, whereas others are regulated by CaM-dependent pathways (2, 41, 42), which might be explained by the expression of different splice variants.

Physiological Significance of Synergistic Gating of Ano1. In cells in which resting V_m is typically between −90 and −30 mV and resting Ca^{2+} is ∼100 nM, Ano1 channel activation requires both depolarization and increased Ca^{2+}. Elevation of Ca^{2+} to the low μM range at hyperpolarized potentials will be ineffective in opening Ano1, as will modest depolarization without a rise in intracellular Ca^{2+}. This dual regulation by Ca^{2+} and V_m makes Ano1 particularly well suited to serve as a feedback regulator of V_m and $[Ca^{2+}]_i$. Because E_{Cl} is dynamically regulated both temporally and spatially in many cells (1), Cl^- fluxes may be inward or outward, depending on local values of E_{Cl}, $[Ca^{2+}]_i$, and V_m. Thus, Ano1 might have a negative or a positive feedback function. This might have important physiological and pathological implications in, for example, the genesis of cardiac arrhythmias, where an outward CaCC current normally participates in repolarization of the cardiac action potential in some species (2). However, under conditions of Ca^{2+} overload, this channel produces transient inward currents, which are arrhythmogenic. Similarly, because Ano1 rectification is regulated by $[Ca^{2+}]$, Ano1 in epithelial cells could mediate secretion or absorption, depending on the interplay of V_m, E_{Cl}, and $[Ca^{2+}]_i$. Thus, the exquisite V_m and Ca^{2+} sensitivity of CaCC channels places these channels in a pivotal position for regulation of cellular excitability.

Experimental Procedures

Electrophysiology. HEK-293 cells were transiently transfected with 0.1–1 μg of mouse Ano1(***a,c***) tagged on the C terminus with EGFP (provided by Dr. Uhtaek Oh, Seoul National University) per 35-mm dish using Fugene-6 (Roche) and patch-clamped 24–72 h later at room temperature (27). Mutations were made by PCR-based mutagenesis (Quickchanger; Agilent) and confirmed by sequencing. Transfected cells were identified by EGFP fluorescence. For whole-cell recording, zero Ca^{2+} pipette solution contained 146 mM CsCl, 2 mM $MgCl_2$, 5 mM EGTA, 10 mM sucrose, and 8 mM Hepes (pH 7.3), adjusted with N-methyl-D-glucamine. High Ca^{2+} pipette solution contained 5 mM Ca^{2+}-EGTA, instead of EGTA (free $Ca2^+$ ∼25 μM). Different free $[Ca^{2+}]$ solutions were made by mixing zero-Ca^{2+} and high-Ca^{2+} solutions. The 126 μM Ca^{2+} was made by adding 0.2 mM $CaCl_2$ to high-Ca^{2+} solution. Br_2-BAPTA [5,5′-dibromo-1,2-bis(2-aminophenoxy)ethane-N,N,N′,N′-tetraacetic acid, 3.5 mM; Invitrogen] was used to make 1-μM to 4-μM free $[Ca^{2+}]$ solutions in some experiments. Standard external solution contained: 140 mM NaCl, 4 mM KCl, 2 mM $CaCl_2$, 1 mM $MgCl_2$, 10 mM glucose, and 10 mM Hepes (pH 7.4). The study of the effects of $[Cl^-]_e$ or $[I^-]_e$ on Ano1 gating used a pipette solution with 2.241 mM $CaCl_2$, 25.241 mM EGTA-TEA, and 50 mM Hepes (pH 7.3) (TEA-OH), and 85 mM D-mannitol (calculated $[Ca^{2+}]$ = 75 nM). High-Cl^- external solution contained 135 mM TEA-Cl, 0.5 mM $CaCl_2$, 20 mM Hepes, and 75 mM D-mannitol. Low-Cl^- external solution contained 0.5 mM $CaCl_2$, 200 mM Hepes, and 45 mM D-mannitol. External solutions with different $[Cl^-]$ concentrations were made by mixing high- and low-Cl^- solutions. Iodide mixtures were made by mixing high-Cl^- external solution with a solution in which Cl^- was replaced by I^-.

Rapid Perfusion. The fast application of Ca^{2+} to excised inside-out patches was performed using a double-barreled theta tubing (1.5 mm o.d.; Sutter Instruments) with a tip diameter of ∼50 μm attached to a piezobimorph on a micromanipulator (43). One barrel was filled with standard zero-$[Ca^{2+}]_i$ solution, and the other barrel was with intracellular solution containing Ca^{2+}. Excised patches were switched between streams by applying ∼100 V to the piezobimorph. The time course of solution exchange across the laminar flow interface was estimated by liquid junction potential measurements to be 0.5 ms (10–90% rise time) for a 10-fold difference in ionic strength (Fig. S3). For BK channel recordings, CsCl was replaced with equimolar KCl.

Data Analysis. Traces were analyzed with Clampfit 9 (Molecular Devices). Conductance (G) from tail currents measured 200 μs after repolarization to −100 mV from various test potentials was normalized to maximum conductance, G_{max}. G/G_{max} vs.V_m curves were fitted to a Boltzmann function with Origin 7 (OriginLab). Results are presented as mean ± SEM.

ACKNOWLEDGMENTS. We thank Uhtaek Oh for helpful discussions and Steve Traynelis and Katie Vance for discussions and technical assistance with fast perfusion. This work was supported by National Institutes of Health Grants GM60448 and EY014852 (to H.C.H.), CONACyT Grants 79897 (to J.A.) and 105457 (to P.P.C.), and an American Heart Association postdoctoral fellowship (to Q.X.).

1. Duran C, Thompson CH, Xiao Q, Hartzell HC (2010) Chloride channels: Often enigmatic, rarely predictable. *Annu Rev Physiol* 72:95–121.
2. Hartzell C, Putzier I, Arreola J (2005) Calcium-activated chloride channels. *Annu Rev Physiol* 67:719–758.
3. Tarran R (2004) Regulation of airway surface liquid volume and mucus transport by active ion transport. *Proc Am Thorac Soc* 1:42–46.
4. Tarran R, et al. (2002) Regulation of murine airway surface liquid volume by CFTR and Ca^{2+}-activated Cl^- conductances. *J Gen Physiol* 120:407–418.
5. Stephan AB, et al. (2009) ANO2 is the cilial calcium-activated chloride channel that may mediate olfactory amplification. *Proc Natl Acad Sci USA* 106:11776–11781.
6. Hengl T, et al. (2010) Molecular components of signal amplification in olfactory sensory cilia. *Proc Natl Acad Sci USA* 107:6052–6057.
7. Rasche S, et al. (2010) Tmem16b is specifically expressed in the cilia of olfactory sensory neurons. *Chem Senses* 35:239–245.
8. Stöhr H, et al. (2009) TMEM16B, a novel protein with calcium-dependent chloride channel activity, associates with a presynaptic protein complex in photoreceptor terminals. *J Neurosci* 29:6809–6818.
9. Large WA, Wang Q (1996) Characteristics and physiological role of the $Ca^{(2+)}$-activated Cl^- conductance in smooth muscle. *Am J Physiol* 271:C435–C454.
10. Duan D (2009) Phenomics of cardiac chloride channels: The systematic study of chloride channel function in the heart. *J Physiol* 587:2163–2177.

11. Liu B, et al. (2010) The acute nociceptive signals induced by bradykinin in rat sensory neurons are mediated by inhibition of M-type K^+ channels and activation of Ca^{2+}-activated Cl^- channels. *J Clin Invest* 120:1240–1252.
12. Miledi R (1982) A calcium-dependent transient outward current in *Xenopus laevis* oocytes. *Proc R Soc Lond B Biol Sci* 215:491–497.
13. Barish ME (1983) A transient calcium-dependent chloride current in the immature *Xenopus* oocyte. *J Physiol* 342:309–325.
14. Yang YD, et al. (2008) TMEM16A confers receptor-activated calcium-dependent chloride conductance. *Nature* 455:1210–1215.
15. Caputo A, et al. (2008) TMEM16A, a membrane protein associated with calcium-dependent chloride channel activity. *Science* 322:590–594.
16. Schroeder BC, Cheng T, Jan YN, Jan LY (2008) Expression cloning of TMEM16A as a calcium-activated chloride channel subunit. *Cell* 134:1019–1029.
17. Romanenko VG, et al. (2010) Tmem16A encodes the Ca^{2+}-activated Cl^- channel in mouse submandibular salivary gland acinar cells. *J Biol Chem* 285:12990–13001.
18. Huang F, et al. (2009) Studies on expression and function of the TMEM16A calcium-activated chloride channel. *Proc Natl Acad Sci USA* 106:21413–21418.
19. Hwang SJ, et al. (2009) Expression of anoctamin 1/TMEM16A by interstitial cells of Cajal is fundamental for slow wave activity in gastrointestinal muscles. *J Physiol* 587: 4887–4904.
20. Rock JR, Futtner CR, Harfe BD (2008) The transmembrane protein TMEM16A is required for normal development of the murine trachea. *Dev Biol* 321:141–149.
21. Rock JR, et al. (2009) Transmembrane protein 16A (TMEM16A) is a Ca^{2+}-regulated Cl^- secretory channel in mouse airways. *J Biol Chem* 284:14875–14880.
22. Arreola J, Melvin JE, Begenisich T (1996) Activation of calcium-dependent chloride channels in rat parotid acinar cells. *J Gen Physiol* 108:35–47.
23. Kuruma A, Hartzell HC (2000) Bimodal control of a $Ca^{(2+)}$-activated $Cl^{(-)}$ channel by different $Ca^{(2+)}$ signals. *J Gen Physiol* 115:59–80.
24. Pifferi S, Dibattista M, Menini A (2009) TMEM16B induces chloride currents activated by calcium in mammalian cells. *Pflugers Arch* 458:1023–1038.
25. Falke JJ, Drake SK, Hazard AL, Peersen OB (1994) Molecular tuning of ion binding to calcium signaling proteins. *Q Rev Biophys* 27:219–290.
26. Cui J, Yang H, Lee US (2009) Molecular mechanisms of BK channel activation. *Cell Mol Life Sci* 66:852–875.
27. Xiao Q, Prussia A, Yu K, Cui YY, Hartzell HC (2008) Regulation of bestrophin Cl channels by calcium: Role of the C terminus. *J Gen Physiol* 132:681–692.
28. Ferrera L, et al. (2009) Regulation of TMEM16A chloride channel properties by alternative splicing. *J Biol Chem* 284:33360–33368.
29. Chao SH, Suzuki Y, Zysk JR, Cheung WY (1984) Activation of calmodulin by various metal cations as a function of ionic radius. *Mol Pharmacol* 26:75–82.
30. Perez-Cornejo P, De Santiago JA, Arreola J (2004) Permeant anions control gating of calcium-dependent chloride channels. *J Membr Biol* 198:125–133.
31. Qu Z, Hartzell HC (2000) Anion permeation in $Ca^{(2+)}$-activated $Cl^{(-)}$ channels. *J Gen Physiol* 116:825–844.
32. Auerbach A, Sigurdson W, Chen J, Akk G (1996) Voltage dependence of mouse acetylcholine receptor gating: Different charge movements in di-, mono- and unliganded receptors. *J Physiol* 494:155–170.
33. Colquhoun D (1998) Binding, gating, affinity and efficacy: The interpretation of structure-activity relationships for agonists and of the effects of mutating receptors. *Br J Pharmacol* 125:924–947.
34. Sánchez-Rodríguez JE, De Santiago-Castillo JA, Arreola J (2010) Permeant anions contribute to voltage dependence of ClC-2 chloride channel by interacting with the protopore gate. *J Physiol* 588:2545–2556.
35. Horrigan FT, Cui J, Aldrich RW (1999) Allosteric voltage gating of potassium channels, I: Mslo ionic currents in the absence of Ca(2+). *J Gen Physiol* 114:277–304.
36. Horrigan FT, Aldrich RW (2002) Coupling between voltage sensor activation, Ca^{2+} binding and channel opening in large conductance (BK) potassium channels. *J Gen Physiol* 120:267–305.
37. Sheridan JT, et al. (2011) Characterization of the oligomeric structure of the $Ca^{(2+)}$-activated Cl^- channel Ano1/TMEM16A. *J Biol Chem* 286:1381–1388.
38. Fallah G, et al. (2011) TMEM16A(a)/anoctamin-1 shares a homodimeric architecture with CLC chloride channels. *Mol Cell Proteom* 10(2):1–10.
39. Tian Y, et al. (2011) Calmodulin-dependent activation of the epithelial calcium-dependent chloride channel TMEM16A. *FASEB J* 25:1058–1068.
40. Das S, et al. (2008) Topology of NGEP, a prostate-specific cell:cell junction protein widely expressed in many cancers of different grade level. *Cancer Res* 68:6306–6312.
41. Arreola J, Melvin JE, Begenisich T (1998) Differences in regulation of Ca^{2+}-activated Cl^- channels in colonic and parotid secretory cells. *Am J Physiol Cell Physiol* 274: C161–C166.
42. Kaneko H, Möhrlen F, Frings S (2006) Calmodulin contributes to gating control in olfactory calcium-activated chloride channels. *J Gen Physiol* 127:737–748.
43. Traynelis SF, Wahl P (1997) Control of rat GluR6 glutamate receptor open probability by protein kinase A and calcineurin. *J Physiol* 503:513–531.